Published in final edited form as:
Adv Funct Mater. 2014 March 26; 24(12): 1772–1780. doi:10.1002/adfm.201301659.

Gold-Coated Fe_3O_4 Nanoroses with Five Unique Functions for Cancer Cell Targeting, Imaging and Therapy

Chunmei Li,
Center for Research at Bio/Nano Interface, Department of Chemistry and Department of Physiology and Functional Genomics, Shands Cancer Center, UF Genetics Institute and McKnight Brain Institute, University of Florida, Gainesville, Florida, 32611-7200, United States; Ministry of Education Key Laboratory on Luminescence and Real-Time Analysis, College of Chemistry and Chemical Engineering, College of Pharmaceutical Science, Southwest University, Chongqing 400715, (P.R. China)

Tao Chen,
Center for Research at Bio/Nano Interface, Department of Chemistry and Department of Physiology and Functional Genomics, Shands Cancer Center, UF Genetics Institute and McKnight Brain Institute, University of Florida, Gainesville, Florida, 32611-7200, United States

Ismail Ocsoy,
Center for Research at Bio/Nano Interface, Department of Chemistry and Department of Physiology and Functional Genomics, Shands Cancer Center, UF Genetics Institute and McKnight Brain Institute, University of Florida, Gainesville, Florida, 32611-7200, United States

Guizhi Zhu,
Center for Research at Bio/Nano Interface, Department of Chemistry and Department of Physiology and Functional Genomics, Shands Cancer Center, UF Genetics Institute and McKnight Brain Institute, University of Florida, Gainesville, Florida, 32611-7200, United States

Emir Yasun,
Center for Research at Bio/Nano Interface, Department of Chemistry and Department of Physiology and Functional Genomics, Shands Cancer Center, UF Genetics Institute and McKnight Brain Institute, University of Florida, Gainesville, Florida, 32611-7200, United States

Dr. Mingxu You,
Center for Research at Bio/Nano Interface, Department of Chemistry and Department of Physiology and Functional Genomics, Shands Cancer Center, UF Genetics Institute and McKnight Brain Institute, University of Florida, Gainesville, Florida, 32611-7200, United States

Cuichen Wu,
Center for Research at Bio/Nano Interface, Department of Chemistry and Department of Physiology and Functional Genomics, Shands Cancer Center, UF Genetics Institute and McKnight Brain Institute, University of Florida, Gainesville, Florida, 32611-7200, United States

Correspondence to: Cheng Zhi Huang, chengzhi@swu.edu.cn; Weihong Tan, tan@chem.ufl.edu.

Supporting Information: Supporting Information is available form the Wiley Online Library or from the author. It includes the nanorose characterization, Dox loading and release, binding and internalization of nanorose-sgc8 to CCRF-CEM and Ramos cells using a confocal fluorescence microscope, cytotoxicity of nanorose-sgc8 to CCRF-CEM and Ramos cells.

Jing Zheng,
Center for Research at Bio/Nano Interface, Department of Chemistry and Department of Physiology and Functional Genomics, Shands Cancer Center, UF Genetics Institute and McKnight Brain Institute, University of Florida, Gainesville, Florida, 32611-7200, United States; Molecular Sciences and Biomedicine Laboratory, State Key Laboratory for Chemo/Biosensing and Chemometrics, College of Chemistry and Chemical Engineering and College of Biology, Collaborative Innovation Center for Chemistry and Molecular Medicine, Hunan University, Changsha 410082, China

Prof. Erqun Song,
Center for Research at Bio/Nano Interface, Department of Chemistry and Department of Physiology and Functional Genomics, Shands Cancer Center, UF Genetics Institute and McKnight Brain Institute, University of Florida, Gainesville, Florida, 32611-7200, United States; Ministry of Education Key Laboratory on Luminescence and Real-Time Analysis, College of Chemistry and Chemical Engineering, College of Pharmaceutical Science, Southwest University, Chongqing 400715, (P.R. China),

Prof. Cheng Zhi Huang, and
Ministry of Education Key Laboratory on Luminescence and Real-Time Analysis, College of Chemistry and Chemical Engineering, College of Pharmaceutical Science, Southwest University, Chongqing 400715, (P.R. China)

Prof. Weihong Tan
Center for Research at Bio/Nano Interface, Department of Chemistry and Department of Physiology and Functional Genomics, Shands Cancer Center, UF Genetics Institute and McKnight Brain Institute, University of Florida, Gainesville, Florida, 32611-7200, United States; Molecular Sciences and Biomedicine Laboratory, State Key Laboratory for Chemo/Biosensing and Chemometrics, College of Chemistry and Chemical Engineering and College of Biology, Collaborative Innovation Center for Chemistry and Molecular Medicine, Hunan University, Changsha 410082, China

Cheng Zhi Huang: chengzhi@swu.edu.cn; Weihong Tan: tan@chem.ufl.edu

Abstract

The development of nanomaterials that combine diagnostic and therapeutic functions within a single nanoplatform is extremely important for molecular medicine. Molecular imaging with simultaneous diagnosis and therapy will provide the multimodality needed for accurate diagnosis and targeted therapy. Here, we demonstrate gold-coated iron oxide (Fe_3O_4@Au) nanoroses with five distinct functions, which integrate aptamer-based targeting, magnetic resonance imaging (MRI), optical imaging, photothermal therapy and chemotherapy into one single probe. The inner Fe_3O_4 core functions as an MRI agent, while the photothermal effect is achieved through near-infrared absorption by the gold shell, causing a rapid rise in temperature and also resulting in a facilitated release of the anticancer drug doxorubicin carried by the nanoroses. Where the doxorubicin is released is monitored by its fluorescent. Aptamers immobilized on the surfaces of the nanoroses enable efficient and selective drug delivery, imaging and photothermal effect with high specificity. The five-function-embedded nanoroses show great advantages in multimodality.

Keywords

nanorose; chemotherapy; photothermal therapy; cancer cells; imaging

1. Introduction

Multifunctional nanomaterials able to integrate both diagnosis and therapy into a single multimodal nanoplatform have emerged as a promising tool for target-specific delivery of imaging and therapeutic agents in biomedical applications in the era of molecular medicine and personalized medicine.[1] Each imaging modality has its own advantages and intrinsic limitations in terms of sensitivity, spatial resolution, and complexity.[1b, 2] Thus, it should be possible to rationally design a platform that combines imaging modalities with high sensitivity, e.g., positron emission tomography (PET) and optical imaging, with other modalities having high spatial resolution, e.g., computed tomography (CT) or MRI, to acquire complementary information, leading to more accurate diagnoses.[1b, 2-3] Combining two therapeutic modalities is also helpful in overcoming serious limitations encountered by each therapy when used alone.[1b, 1d, 4] For instance, chemotherapy, an important modality in cancer treatment, is limited by drug resistance and toxic side effects, making targeted drug delivery and controlled drug release major challenges. However, based on the attractive photothermal effect of some plasmonic nanomaterials, the combination of photothermal agents and chemotherapy is an encouraging approach to achieve enhanced cancer killing efficiency through synergistic effects.[4d, 5] Further, under these conditions, smaller drug doses may be sufficient for the desired therapeutic outcome, since cells exposed to higher temperature are more susceptible to certain chemotherapy drugs.

To improve specificity, recognition elements, such as folic acids,[6] peptides,[7] and, of particular interest, aptamers,[8] are commonly incorporated for targeted delivery. Aptamers are single-stranded oligonucleotides generated from an *in vitro* selection process called SELEX (Systematic Evolution of Ligands by EXponential enrichment). They can bind to their targets, including small molecules, proteins, and even intact cells and tissues, with excellent specificity and high affinity.[9] Significant advantages, such as ease of synthesis and surface modification, long-term stability, lack of immunogenicity, and rapid tissue penetration, make aptamers ideal candidates for molecular recognition, [10] drug delivery, [11] cancer diagnosis, and therapy.[12]

Several aptamer conjugates functionalized with various nanomaterials have already been reported. These nanocarriers integrate such capabilities as fluorescence imaging, MRI, and the photothermal effect into one single platform.[13] Building on this design, the present paper describes a novel nanoplatform performing five distinct functions synergistically and effectively. To accomplish this, we have prepared gold-coated iron oxide (Fe_3O_4@Au) nanoroses with several excellent features, including biocompatibility, NIR absorption, and superparamagnetic properties.[14] Based on these properties, the nanoroses can be used as both photothermal agents for photothermal therapy and contrast agents for MRI. They can also be easily conjugated with aptamers *via* thiolate bonding, for example, sgc8 aptamers, which specifically recognize CCRF-CEM leukemia cells, as a model for targeted imaging and therapy. Additionally, the chemotherapeutic agent doxorubicin (Dox) can be

intercalated into the GC base pairs in the extended part of the aptamers as a drug delivery platform.[8b, 12c, 15] By combining these capabilities, we have developed a drug-loaded Fe_3O_4@Au nanorose platform with five distinct functions for simultaneous imaging and therapy: targeting with aptamers, dual molecular imaging (MRI/optical imaging) and dual therapy (photothermal/chemotherapy) (Figure 1).

2. Results and Discussion

2.1. Synthesis and Characterization

As shown in Figure 2, this five-function nanorose contains four components: 1) the Fe_3O_4@Au nanorose, which acts as both a photothermal agent and an MRI contrast agent; 2) surface modification with a carboxylic acid-PEG derivative (SH-PEG-COOH) and a capture probe, 5′-$(GCT)_7$-T_{10}-SH-3′, for Dox loading and hybridization with sgc8 aptamer; 3) sgc8 aptamer, modified with a desired fluorophore at the 3′-end and a 21-base $(AGC)_7$ extension at the 5′-end, to target CCRF-CEM cells and act as a carrier for Dox and 4) Dox, acting as both a chemotherapeutic agent and an optical imaging agent, which is loaded through both intercalation into the extended GC base pairs and electrostatic interaction with the carboxyl groups on the nanorose surface.[12c, 16] Dox loading capacity is significantly enhanced by fusing the $(AGC)_7$ repeating oligonucleotide to the original sgc8 aptamer.[17] Two PEG units are incorporated between the sgc8 aptamer and the $(AGC)_7$ extended sequence in order to reduce the steric effects of binding to target cells and to locate the fluorophore away from the gold surface to allow further flow cytometry study (Figure 2). The intercalation of Dox into the nanorose, which also serves as a photothermal agent, results in a single multifunctional nanostructure integrating simultaneous photothermal cell killing and drug release (photothermal/chemotherapy) for enhanced antitumor killing efficiency and reduced toxic side effects. In addition, dual modality imaging, i.e., optical imaging and MRI, can provide complementary information for early and accurate cancer diagnosis, as well as real-time therapeutic drug monitoring.

Nanoroses were prepared following the slightly modified protocol reported previously.[14, 18] The Fe_3O_4 nanoparticle cores were synthesized in the presence of dextran. Then, nanoroses were formed by the reduction of $HAuCl_4$ onto the surfaces of Fe_3O_4 with hydroxylamine as a seeding agent and dextrose as a mild reducing agent. Transmission electron microscopy (TEM) images showed that the Fe_3O_4 core was small in size (estimated to be 3-5 nm in diameter) (Figure 3a) and that the nanorose with flower-like cluster shape was around 70 nm in diameter (Figure 3b). The hydrodynamic diameter distribution determined by dynamic light scattering (DLS) in Figure 3c showed that the average nanorose diameter was 78.4 ± 6.4 nm, which was consistent with the TEM result. It has been reported that the gold shell thickness is ∼1-3 nm.[14, 18] The nanorose stayed homogenous for at least 6 days at 4 °C and can be well dispersed after sonication. The molar concentration of the nanoroses was calculated as reported previously.[18] A representative energy-dispersive X-ray spectroscopy [19] line scan across the nanorose during scanning transmission electron microscope (STEM) imaging confirmed that Fe and O were present throughout the cluster diameter and that Au was on the outer surface (Figure 3d, e). The Au/Fe mass ratio was about 13:1 based on the EDS spectrum, which was higher than that

obtained from inductively coupled plasma-atomic emission spectroscopy (ICP-AES) (4.5:1), as a consequence of the existence of uncoated Fe_3O_4 nanoparticles. The UV-Vis-NIR absorption spectrum in Figure 3f showed that the nanorose solution has an obvious absorption in the NIR window at 805 nm, which is in the wavelength range for maximum depth of penetration in tissue. The aqueous nanorose solution was dark blue (inset in Figure 3f), and its temperature can be increased to around 50 °C with an 810 nm continuous wave laser irradiation at 1.3 W/cm^2 for 10 min (Figure S1), indicating that nanoroses can efficiently convert light to heat for photothermal therapy. The potential of nanoroses as T_2-based contrast agents for MRI was demonstrated with 1) transverse relaxivity r_2 of 80 $mM^{-1}s^{-1}$ (Figure S2a) and 2) dramatically decreased signal intensity of the T_2-weighted MRI with increasing Fe concentration (Figure S2b).

2.2. Surface modification of nanoroses for drug delivery and cancer cell targeting

As shown in Figure 2, the surfaces of nanoroses were modified with SH-PEG-COOH *via* gold-thiol bonds, which can stabilize the particles and enable the loading of anticancer drug Dox *via* electrostatic interactions. A capture probe with SH modification at the 3′-end was simultaneously conjugated on the nanoroses to hybridize with sgc8 for targeting and also to load Dox through intercalation into GC base pairs in the extended part of the aptamers (Table S1, SI). The results showed that each nanorose possessed about 125 ± 4 sgc8, providing the possibility of multivalent effect when binding to target cells. Dox loading onto the nanorose-sgc8 hybrid (nanorose-sgc8-Dox) was confirmed by monitoring the fluorescence quenching of Dox. Based on the titration data (Figure S3), we estimated that 48 ± 2 % of Dox was bound to the carboxyl group by electrostatic interactions and that 52 ± 3 % was intercalated into the GC base pairs. However, it's also possible that Dox can be adsorbed directly onto the gold surface due to hydrophobic interaction, that is, the interaction between the aromatic rings with the gold surface. As calculated, the loading efficiency of Dox (the amount of Dox loaded divided by the amount of nanorose-sgc8 used) was estimated to be about 498 μg Dox mg^{-1} (49.8 wt %) for nanorose-sgc8. DLS and zeta potential tests (Figure S4), also confirmed successful aptamer conjugation and efficient Dox loading on each nanorose. The stability of the nanorose-sgc8 in physiological environments, such as serum-containing cell culture media was tested, indicating that it can be stable against degradation and digestion of nuclease as a result of the high oligonucleotide loading. [20]

To demonstrate that the conjugated aptamer maintains its binding affinity and specificity, the binding of nanorose-sgc8 toward target and control cancer cells was studied by flow cytometry. It has been reported that sgc8 can specifically bind to cell membrane receptor protein tyrosine kinase (PTK 7) with high affinity (*K*d in the nM rang).[9c, 21] CCRF-CEM cells (acute lymphoblastic leukemia T-cells), with highly expressed PTK 7 on their cell membranes, were chosen as target cancer cells, while Ramos cells (acute lymphoblastic leukemia B-cells), with no expression of PTK7 on the cell membrane, were used as negative control cells. In Figure 4a, a stronger fluorescence signal was observed for CCRF-CEM cells treated with nanorose-sgc8 (with 165 nM sgc8) than with free sgc8 (200 nM), indicating that a multivalent-mediated enhancement in affinity arises when multiple aptamers on the surface of a nanoparticle carrier simultaneously bind to the receptors on the cell membrane.

This significant fluorescence enhancement was also monitored using confocal fluorescence microscopy (Figure S5a,c). No significant fluorescence change was observed for a random library (Lib) sequence or Ramos cells, further confirming the specific recognition of the nanorose-sgc8 for CCRF-CEM cells (Figure 4b; Figure S5b,d). A bar graph in Figure 4c was used to summarize the mean fluorescence calculated from Figure 4a and Figure 4b.

To confirm that nanorose-sgc8 can be internalized into target cells for further therapy application, an internalization study was carried out at 37 °C with trypsin treatment. It is known that trypsin treatment can be used to remove the surface binding of sgc8 with target cells.[22] For CCRF-CEM cells, sgc8 was internalized prior to the addition of trypsin at 37 °C, but the surface-bound sgc8 was removed by trypsinization at 4 °C. The fluorescence signal was stronger at 37 °C than that at 4 °C after trypsin treatment, showing that nanorose-sgc8 was internalized at 37 °C. The bar graph in Figure 4f indicated that Ramos cells have neglectable binding with nanorose-sgc8 no matter at 4 °C or 37 °C. It has been reported that free sgc8 can be internalized and delivered into the lysosomes as a result of PTK7-mediated endocytosis.[22] To further evaluate whether nanorose-sgc8 could enter the lysosomes in a manner similar to free sgc8, a red dye, tetramethylrhodamine (TAMRA), and a green dye, LysoSensor, a pH-dependent lysosome marker, were used to label the aptamer and lysosomes of CCRF-CEM cells, respectively, for a colocalization study. The green fluorescence for LysoSensor and the red fluorescence for sgc8 or nanorose-sgc8 overlapped well and produced the merged yellow fluorescence inside the CCRF-CEM cells, indicating that both sgc8 and nanorose-sgc8 were internalized by the cell through the endocytosis process (Figure S6). Consistent with the flow cytometry results, stronger red fluorescence was observed for cells incubated with nanorose-sgc8 (Figure S6a) compared to a higher concentration of free sgc8 (Figure S6b), indicating an improved uptake efficiency of nanorose-sgc8 by CCRF-CEM cells. To evaluate Dox release kinetics, we incubated nanorose-sgc8-Dox in phosphate buffered saline (PBS) buffer at different pH values (pH 5.0 and 7.4) and different temperatures (25°C, 37°C, 65°C). The release of Dox was pH- and temperature-dependent, with faster release in acidic environments and at higher temperatures (Figure S7). It has been reported that physically bound Dox is released faster at mildly acidic pH values than at neutral pH, as a consequence of weakened binding between Dox and the partially neutralized carboxyl groups.[23] In addition, Dox intercalated into GC base pairs in the extended aptamers is released faster *via* degradation of nucleotides by serum nucleases and dehybridization of aptamer at high temperature.[8b], [12c] Based on these findings, we propose that Dox bound to aptamers enters the lysosome of CCRF-CEM cells, where it is rapidly released at low pH. A further rapid release of Dox may be observed after exposure to laser irradiation, which increases the temperature by the photothermal effect.[24]

2.3. Nanorose complex for chemotherapy and photothermal therapy

To assess the specificity of our targeted drug delivery system, we investigated the *in vitro* cytotoxicity of nanorose-sgc8-only, Dox-only, and nanorose-sgc8-Dox for two leukemia cell lines. Both CCRF-CEM and Ramos cells showed high cell viability (above 93%) after incubation with a series of concentrations of nanorose-sgc8-only, indicating that our probe has excellent biocompatibility (Figure S8). Dox-only and nanorose-sgc8-Dox exhibited

dose-dependent cytotoxicity behavior to CCRF-CEM cells, as well as Ramos cells. Figure 5ab shows that the inhibition concentration (IC_{50}) of nanorose-sgc8-Dox to CCRF-CEM cells was 1.1 μM, which is quite similar to that for Dox-only (IC_{50}=1.2 μM), demonstrating that nanorose-sgc8-only did not affect the killing efficiency of Dox to CCRF-CEM cells. For Ramos cells, the cell viability of 47.1±3.8 % with Dox-only treatment (3.0 μM) increased to 87.6±2.5 % with nanorose-sgc8-Dox treatment. This can be attributed to the lack of PTK7 expression on the surface of Ramos cells, indicating that nonspecific uptake of Dox was minimized by the formation of a stable nanorose-sgc8-Dox conjugate. The cytotoxicity results demonstrated that the drug delivery system has excellent selectivity compared to conventional chemotherapy using Dox-only, an important benefit for reducing the side effects of chemotherapy.

To prove that nanorose-sgc8 can also be used for photothermal therapy, CCRF-CEM and Ramos cells incubated with nanorose-sgc8 were exposed to 810 nm laser illumination at 1.3 W/cm^2 for 10 min. Irradiation of CCRF-CEM cells with nanorose-sgc8 increased the temperature to 51.3 °C, while Ramos cells incubated with nanorose-sgc8 only reached 35.7 °C (Figure S9). Cell death after treatment with nanorose-sgc8-only, Dox-only, and nanorose-sgc8-Dox, with or without laser irradiation, was determined by using propidium iodide (PI) dye to stain the dead cells, followed by flow cytometry monitoring (Figure 5cd). A control experiment by directly illuminating CCRF-CEM cells alone without Dox or nanorose-sgc8 treatment for different irradiation time was conducted, and negligible toxicity was observed, demonstrating the laser biocompatibility (Figure 5cd, Figure S9). After Dox treatment, CCRF-CEM cell viability decreased to 59 ± 5.4 %, while laser irradiation did not affect the viability significantly (52 ± 0.9 %). Without irradiation, the nanorose-sgc8 hybrid showed excellent biocompatibility and was not toxic to either CCRF-CEM or Ramos cells (Figure S8). However, almost half of the CCRF-CEM cells were killed by nanorose-sgc8 after laser illumination by the specific binding of nanorose-sgc8 to target cells, coupled with photothermal effect. In addition, exposure to NIR irradiation increased the rate of Dox release from the nanorose-sgc8-Dox complex based on the higher temperature. As shown in Figure 5c, when combined with photothermal therapy, 0.8 μM of Dox released from nanorose-sgc8-Dox was sufficient to kill about 71 ± 0.7 % of the CCRF-CEM cells, while 2.0 μM of free Dox was needed to reach the same killing efficiency (Figure 5a). The synergistic effect between Dox and NIR irradiation has been well demonstrated through the addition of NIR photothermal agents to cells subjected to Dox treatment, showing enhanced Dox toxicity *via* NIR irradiation.[5a, 25] Therefore, smaller drug doses are sufficient to achieve the desired therapeutic outcome under hyperthermic conditions, so that nonspecific toxicity and side effects can be minimized.

The specificity of the treatment was investigated by incubating control cells (Ramos cells) with free Dox, nanorose-sgc8 and nanorose-sgc8-Dox under the same conditions as those for CCRF-CEM cells (Figure 5d). Cell viability of Ramos cells was higher than 85 ± 4 %, even with laser irradiation, after nanorose-sgc8-Dox treatment. These results demonstrate that nanorose-sgc8-Dox shows minimal toxicity to control cells based on the specificity of sgc8 aptamer. Taken together, the data indicate that treatment of CCRF-CEM cells with nanorose-sgc8-Dox followed by NIR laser irradiation has significantly greater cytotoxic

effect, compared to the treatment with nanorose-sgc8-only (photothermal therapy) or Dox-only (chemotherapy). This enhanced antitumor effect with nanorose-sgc8-Dox plus laser irradiation can be attributed to both the cytotoxic effect of Dox released from nanorose-sgc8-Dox and the photothermal effect generated by the nanoroses under NIR laser exposure.

2.4. Nanorose complex for optical imaging and MRI

The specific binding and release of Dox from nanorose-sgc8-Dox was further studied by co-localization with the LysoSensor using confocal fluorescence microscopy. From Figure 6a, it can be seen that the green fluorescence from the LysoSensor and the red fluorescence from the released Dox overlapped well, producing a yellow signal inside the CCRF-CEM cells. This result demonstrated that nanorose-sgc8-Dox can enter the cells through endocytosis process and reside in their lysosomes. Therefore, the dissolution of nanorose-sgc8-Dox in acidic cellular lysosomes became a trigger factor for Dox release in our system. A very weak red signal was observed in Ramos cells (Figure 6b), which resulted from negligible nonspecific binding. These results additionally support our nanorose-sgc8-Dox as a highly promising platform for selective and comprehensive cancer cell diagnosis and therapy.

Since most biological samples exhibit virtually no magnetic background, high sensitivity can be achieved using magnetic nanoparticles for MRI detection of biological samples, even without purification. Hence, an effective magnetic relaxation switch (MRSw) was developed based on cluster formation or dissociation when MNPs bind to specific targets, which leads to a change in the transverse or spin-spin relaxation time (T_2)[26] We investigated the potential of using nanorose-sgc8 for specific detection of target cancer cells by T_2 measurement and MRI. When the nanorose-sgc8 hybrids bind to CCRF-CEM cells through the specific interaction between receptors on the cell membrane and aptamers on the nanorose surface, clusters formed on the cell membrane, resulting in coupling of the magnetic spin moment and decreased T_2. Figure 7a shows a larger ΔT_2 caused by nanorose-sgc8 with CCRF-CEM cells, compared to nanorose-sgc8 with Ramos cells, resulting from the overexpressed PTK7 receptors on CCRF-CEM cells. Next, T_2-weighted MRI images were further taken after CCRF-CEM and Ramos cells were treated with different concentrations of nanorose-sgc8. Consistent with the relaxation data, Figure 7b shows that much darker images were observed for the left column (CCRF-CEM cells) for all three concentrations of nanorose-sgc8. These results indicate that nanorose-sgc8 has the potential to be used as a selective and effective image contrast agent for MRI application.

3. Conclusions

In summary, we have developed a five-function sgc8 aptamer-conjugated nanorose to serve not only as an anticancer drug carrier, but also as an efficient photothermal therapy agent to kill target cancer cells by direct heat, thereby also facilitating rapid drug release. Thus, the killing efficiency can be improved with reduced drug doses. Our design offers several attractive features: (1) five different functions synergistically integrated into a single platform by a nanorose about 70 nm in diameter; (2) enhanced specific binding and improved cellular uptake by multivalent effect; (3) minimum nonspecific toxicity and side effects based on a lower dosage of chemotherapy drugs when combined with photothermal

therapy. The combination of dual-modality MRI and optical imaging has the potential to improve the specificity of cancer cell diagnosis and facilitate therapeutic drug monitoring. The amounts of imaging agent, photothermal agent or drug loaded into the system can be adjusted to perform each function synergistically and effectively. It is expected that this versatile theranostic system will have wide biomedical applications and may be particularly useful for cancer therapy.

4. Experimental Section

Materials—Iron (II) chloride tetrahydrate, Iron (III) chloride hexahydrate, Gold (III) chloride trihydrate, Doxorubicin hydrochloride and Dextran (Mr ~40,000) were all purchased from Sigma-Aldrich. Hydroxylamine Hydrochloride was ordered from Fisher Scientific.

Nanorose Synthesis—The nanoroses were prepared using methods described previously with slight modifications [14, 18]. First, 3-5 nm Fe_3O_4 nanoparticles were synthesized by the co-precipitation method. An aqueous dextran solution (15 mL, 15%, w/w) was titrated with NH_4OH solution (8mL, >25%, w/w) to pH 11.7. Then a freshly prepared aqueous solution (10mL) containing $FeCl_3{\cdot}6H_2O$ (1.5 g) and $FeCl_2{\cdot}4H_2O$ (0.64 g) was gradually injected into the dextran solution with magnetic stirring after passing through a hydrophilic 0.22 um filter. After stirring for 0.5 h at room temperature, the black suspension was centrifuged at 10,000 rpm for 20 min to remove the large aggregates. Fe_3O_4 nanoparticles in the supernatant solution were collected using an external magnetic field. The concentration of Fe_3O_4, as determined from ICP-AES, was 240μg/mL. Nanoroses were formed by the reduction of $HAuCl_4$ onto the Fe_3O_4 nanoparticles with hydroxylamine as a seeding agent. In brief, the as-prepared dextran-coated Fe_3O_4 solution (0.5 mL) was mixed with DI water (3.5 mL). A hydroxylamine seeding agent (100 μL, 1%, w/w)) and dextrose (0.5 g) as a mild reducing agent were added, and stirring was continued for 15 min at room temperature. Then NH_4OH solution (50 μL, 7%, w/w) was added to the Fe_3O_4 dispersion to tune the pH to 9.0. Every 10 min, an aliquot of $HAuCl_4$ aqueous solution (100 μL, 6.348 mM) was added to the stirred dispersion, until a total of 300 μL of $HAuCl_4$ had been added. The color gradually changed from brown to dark brown during the three aliquot additions. Subsequently, the dense Fe_3O_4@Au particles were separated from the less dense uncoated particles by centrifugation at 8000 rpm for 6 min. The supernatant was decanted, and the nanoroses were redispersed in aqueous dextran solution (5%, w/w) by sonication for 10 min. The centrifugation and redispersion steps were repeated five times to remove the uncoated Fe_3O_4 nanoparticles, then two more times with DI water as dispersant to remove excess dextran molecules. The purified particles were redispersed in Tris-HCl solution (2mL, 10mM, pH 7.4). The hydrodynamic diameters of nanoroses were determined by dynamic light scattering (DLS) (Microtrac Nanotrac™ Ultra). Zeta potential (Zetaplus, Zeta Potential Analyser, Brookhaven Instruments Co.) was used to characterize the surface charge of the nanoroses. Energy-dispersive spectroscopy (EDS) line scan coupled with scanning transmission electron microscopy (STEM) from one nanorose identified the presence of Au and Fe. STEM and EDS were performed on a field emission JEOL JEM-2010F transmission

electron microscope equipped with an Oxford INCA EDS system. EDS line scan was taken with the microscope in STEM mode at 200 kV accelerating voltage.

DNA Synthesis—All DNA sequences (see Supplementary Table 1) were synthesized on an ABI 3400 DNA/RNA synthesizer (Applied Biosystems, Foster City, CA, USA). The aptamer with fluorescein isothiocyanate (FITC) labeling was used for flow cytometry, while the aptamer with tetramethylrhodamine (TAMRA) labeling was used for the study of binding and internalization of nanorose-sgc8 using confocal fluorescence microscopy. Other experiments were carried out using the aptamer without dye labeling. The aptamers with and without FITC labeling were deprotected in AMA solution (ammonium hydroxide : 40% aqueous methylamine = 1:1) (2.5 mL) at 65 °C for 30 min. The TAMRA-labeled aptamer was deprotected in TAMRA deprotection solution (methanol : *tert*-butylamine : water = 1 : 1 : 2) (3 mL) at 65°C for 4 h. Then the solution was transferred to 15 mL centrifuge tubes and mixed with NaCl (250 μL, 3.0 M) and cold ethanol (6.0 mL), followed by a 30 min precipitation in a -20°C freezer. The precipitated DNA oligomers were collected by centrifugation and dissolved in triethylammonium acetate (TEAA) (400 μL, 0.1 M). They were further purified using a reversed-phase high-pressure liquid chromatography (HPLC) (ProStar, Varian, Walnut Creek, CA, USA) with a C_{18} column and acetonitrile-TEAA solvent. Finally, the concentrations of these DNA oligomers were determined by measuing their absorbance at 260 nm with a UV-1800 spectrophotometer (Shimadzu, Japan).

Conjugation of sgc8 Aptamers to Nanoroses—First, thiol-functionalized capture probe and SH-PEG-COOH (Nanocs, MW 3400) were conjugated to the nanoroses following a slightly modified method in the literature [27]. Before conjugation, thiol-modifed capture probe (1.0 mM) was activated by TCEP (1.0 mM, freshly prepared) in acetate buffer (50 mM, pH 5.2) for 1 h at room temperature. SH-PEG-COOH (100μL, 10 mM) and activated thiol-functionalized capture probe (40 μL, 1.0 mM) were added to nanorose solution (2 mL, 49.5 nM) with gentle shaking by hand. The mixture was magnetically stirred at room temperature for at least 16 h. Then Tris acetate (60 μL, 500 mM, pH 8.2) buffer was added dropwise to the solution with gentle hand shaking, followed by dropwise addtion of NaCl (600 μL, 1.0 M). The solution was sonicated for 15 s and then stored at room temperature for 24 h. The free capture probe and SH-PEG-COOH were removed by centrifugation at 14000 rpm for 5 min, and the nanoroses were redispersed in 2 mL Tris-Mg buffer (10 mM Tris-HCl, pH 7.4, containing 100 mM NaCl, 10 mM KCl and 10 mM $MgCl_2$). The resulting nanoroses were then hybridized with extended sgc8 aptamer (40 μL, 1.0 mM) by initally heating the solution to 90 °C for 5 min, followed by incubating at room temperature for 1 h. Unreacted sgc8 was removed by centrifugation at 14000 rpm for 5 min, and nanorose-sgc8 hybrids were redispersed in Tris-HCl buffer (2 mL, pH 7.4).

Dox Loading of Nanorose-sgc8—The maximum achievable loading of Dox onto nanorose and nanorose-sgc8 (both modifed with SH-PEG-COOH) was determined by measuring the unloaded Dox fluorescence in the supernatant. Serial concentrations of nanorose and nanorose-sgc8 (0, 0.16, 0.4, 1.6, 4.0 nM) were added to a fixed concentration of Dox (5.5 μM) with PBS buffer pH 7.4 and incubated at room temperature for 10 min with gentle shaking. The unloaded Dox was removed by centrifugation at 10,000 rpm for 3 min.

The concentration of unloaded Dox in the supernatant was calculated from the emission intensity of Dox at 590 nm with excitation at 480 nm, using a Fluorolog-3 spectrofluorometer (Jobin Yvon Horiba).

Dox Release Kinetics—The release of Dox from the nanorose-sgc8-Dox complex was conducted by incubating nanorose-sgc8-Dox in PBS buffers with different pH values (pH = 5.0, 7.4) at different temperatures (T = 25 °C, 37°C, 65°C). At the indicated times, the particles were collected by centrifugation, and the supernatant was removed for fluorescence analysis and replaced with fresh buffer. The amount of Dox released was accumulated by determining the fluorescence emission of the supernatant at 590 nm at selected time intervals.

Cell Culture—CCRF-CEM (CCL-119 T-cell, human acute lymphoblastic leukemia) and Ramos (CRL-1596, B-cell line, human Burkitt's lymphoma) were cultured in RPMI 1640 medium (American Type Culture Collection) with 10% heat inactivated fetal bovine serum (FBS, Invitrogen, Carlsbad, USA) and penicillin-streptomycin (100 IU/mL, GIBCO) at 37 °C under a 5% CO_2 atmosphere. The cell density was determined using a hemocytometer (Hausser Scientific) and a microscope (Olympus).

Flow Cytometry Analysis—Flow cytometry analysis was performed on a FACScan cytometer (Becton Dickinson Immunocytometry Systems, San Jose, CA, USA) to demonstrate the specific targeting of nanorose-sgc8 to CCRF-CEM cells. The binding affinities of free sgc8 and nanorose-sgc8 functionalized with FITC dye were determined by incubating CCRF-CEM or Ramos cells (1×10^6 cells/mL) with various concentrations of sgc8 and nanorose-sgc8 in a 200 μL binding buffer [Dulbecco's PBS with calcium chloride and magnesium chloride (Sigma), containing glucose (4.5 g/L), $MgCl_2$ (5 mM), yeast tRNA (Sigma, 0.1 mg/mL) and BSA (Fisher Scientific, 1.0 mg/mL)] on ice for 30 min in dark. Cells were washed twice with 1 mL washing buffer [Dulbecco's PBS with calcium chloride and magnesium chloride (Sigma), containing glucose (4.5 g/L), $MgCl_2$ (5 mM)], suspended in binding buffer (200 μL) and subjected to flow cytometry analysis by counting 10,000 events. A green laser at 488 nm was used as the excitation source, and the FITC-labeled random ssDNA library was used as a negative control. To study the internalization of free sgc8 and nanorose-sgc8, CCRF-CEM or Ramos cells (1×10^6 cells/mL) were first incubated with various concentrations of sgc8 and nanorose-sgc8 in binding buffer (200 μL) at 37 °C for 2 h with a 5% CO_2 atmosphere, then washed with washing buffer twice. Then cells were incubated with trypsin (500 μL, 0.05%)/EDTA (0.53 mM) in Hank's Balanced Salt Solution (HBSS) at 37 °C for 10 min. After incubation, FBS (50 μL) was added to quench the function of trypsin, and the cells were washed with washing buffer once again and suspended in binding buffer (200 μL) for flow cytometric analysis.

Confocal Imaging—To investigate the specific binding and internalization of free sgc8 and nanorose-sgc8 toward different cell lines by confocal imaging, the aptamers were labeled with TAMRA dye. However, for the colocalization study of Dox release, aptamers without dye labeling were used. All cellular fluorescence images were collected on an Olympus FV 500-IX81 confocal microscope (Olympus, Center Valley, PA, USA), with a

60× oil-dispersion objective. A 488 nm argon laser was used as the excitation source for FITC dye, and a 543 nm argon laser was used for the excitation of TAMRA dye or Dox. For the specific binding test, the treatment steps for cell incubation were the same as those described for the flow cytometry analysis. For the colocalization study of internalization or Dox release toward different cell lines, free sgc8, nanorose-sgc8, or nanorose-sgc8-Dox was incubated with CCRF-CEM or Ramos cells (1×10^6 cells/mL) in binding buffer (200 μL) at 37 °C for 2 h with a 5% CO_2 atmosphere. Five μM LysoSensor was added for specific staining of the lysosomes of cancer cells during the last 0.5 h of the 2 h incubation. The cells were then washed twice with washing buffer, resuspended in binding buffer (200 μL), and subjected to confocal fluorescence microscopy.

Cytotoxicity Assay—The cytotoxicity of free Dox, nanorose-sgc8 and nanorose-sgc8-Dox to CCRF-CEM and Ramos cells before and after laser irradiation was evaluted using a FACScan cytometer. CCRF-CEM or Ramos cells (1×10^6 cells/mL) were first incubated with various concentrations of Dox-only, nanorose-sgc8-only or nanorose-sgc8-Dox in binding buffer (200 μL) at 37 °C for 2 h with a 5% CO_2 atmosphere, then washed twice with washing buffer. Cells were then exposed to 810 nm laser illumination for 10 min and returned to the incubator for another 48 h. Then cells were stained with propidium iodide (PI; Invitrogen, Carlsbad, CA, USA) at room temperature for 15 min to test cell viability. Dead cells, which can accumulate the dye and show red fluorescence, were determined by flow cytometric analysis. The cell viability was determined by comparing cells treated with Dox, nanorose-sgc8 and nanorose-sgc8-Dox with the corresponding untreated controls.

Photothermal Therapy—The nanoroses absorb in the NIR at 805 nm, which is close to the laser wavelength at 810 nm. Temperature curves were recorded in real time with a COHERENT Quarto-FAP system, while cells were illuminated with an 810 nm continuous wave laser at 1.3 W/cm^2 for 10 min.

Relaxation Time Measurement and Magnetic Resonance Imaging—The spin-spin relaxation times (T_2) were measured at 1.4 T by a standard Carr-Purcell-Meiboom-Gill Sequence on a benchtop Mninispec mq60 TD-NMR contrast agent analyzer (Minispec, Bruker, Germany) operating at 37 °C. Nanoroses-only and nanorose-sgc8 with CCRF-CEM or Ramos cells (1×10^6 cells/mL) were incubated on ice for 30 min in binding buffer (250 μL). Then all samples were transferred to NMR sample tubes and subjected to T_2 relaxation measurements, without any further washing steps. T_2-weighted MRI images were acquired on a 4.7 T/200 MHz MRI spectrometer (Bruker Optics, Billerica, MA), following the same treatment steps as performed for the T_2 relaxation measurements.

Supplementary Material

Refer to Web version on PubMed Central for supplementary material.

Acknowledgments

We thank Dr. Kathryn Williams for editing the manuscript and John W. Munson in the Center for Enviroment and Human Toxicology (CEHT) at the University of Florida for laser support. C.M.L. received financial support from the China Scholarship Council (CSC). This work is supported by grants awarded by the National Key Scientific

Program of China (2011CB911000), the Foundation for Innovative Research Groups of NSFC (Grant 21221003), China National Instrumentation Program 2011YQ03012412 and by the National Institutes of Health (GM079359 and CA133086).

References

1. a) Louie A. Chem Rev. 2010; 110:3146. [PubMed: 20225900] b) Lee DE, Koo H, Sun IC, Ryu JH, Kim K, Kwon IC. Chem Soc Rev. 2012; 41:2656. [PubMed: 22189429] c) Jennings LE, Long NJ. Chem Commun. 2009:3511.d) Kelkar SS, Reineke TM. Bioconjugate Chem. 2011; 22:1879.
2. Bardhan R, Chen W, Perez-Torres C, Bartels M, Huschka RM, Zhao LL, Morosan E, Pautler RG, Joshi A, Halas NJ. Adv Funct Mater. 2009; 19:3901.
3. a) Zhou T, Wu B, Xing D. J Mater Chem. 2012; 22:470.b) Yin M, Li Z, Liu Z, Ren J, Yang X, Qu X. Chem Commun. 2012; 48:6556.c) Santra S, Kaittanis C, Grimm J, Perez JM. small. 2009; 5:1862. [PubMed: 19384879]
4. a) Ta HT, Dass CR, Larson I, Choong PFM, Dunstan DE. Biomaterials. 2009; 30:4815. [PubMed: 19505719] b) Wang J, Zhu G, You M, Song E, Shukoor MI, Zhang K, Altman MB, Chen Y, Zhu Z, Huang CZ, Tan W. ACS Nano. 2012; 6:5070. [PubMed: 22631052] c) Wang T, Zhang L, Su Z, Wang C, Liao Y, Fu Q. ACS Appl Mater Interfaces. 2011; 3:2479. [PubMed: 21604817] d) Liu H, Chen D, Li L, Liu T, Tan L, Wu X, Tang F. Angew Chem Int Ed. 2011; 50:891.
5. a) Zhang W, Guo Z, Huang D, Liu Z, Guo X, Zhong H. Biomaterials. 2011; 32:8555. [PubMed: 21839507] b) Park H, Yang J, Lee J, Haam S, Choi IH, Yoo KH. ACS Nano. 2009; 3:2919. [PubMed: 19772302] c) Zhang Z, Wang L, Wang J, Jiang X, Li X, Hu Z, Ji Y, Wu X, Chen C. Adv Mater. 2012; 24:1418. [PubMed: 22318874]
6. Santra S, Kaittanis C, Santiesteban OJ, Perez JM. J Am Chem Soc. 2011; 133:16680. [PubMed: 21910482]
7. Pearce TR, Shroff K, Kokkoli E. Adv Mater. 2012; 24:3803. [PubMed: 22674563]
8. a) Kolishetti N, Dhar S, Valencia PM, Lin LQ, Karnik R, Lippard SJ, Langer R, Farokhzad OC. Proc Natl Acad Sci USA. 2010; 107:17939. [PubMed: 20921363] b) Luo YL, Shiao YS, Huang YF. ACS Nano. 2011; 5:7796. [PubMed: 21942498]
9. a) Fang X, Tan W. Accounts of Chem Res. 2009; 43:48.b) Shangguan D, Li Y, Tang Z, Cao ZC, Chen HW, Mallikaratchy P, Sefah K, Yang CJ, Tan W. Proc Natl Acad Sci USA. 2006; 103:11838. [PubMed: 16873550] c) Tang Z, Shangguan D, Wang K, Shi H, Sefah K, Mallikratchy P, Chen HW, Li Y, Tan W. Anal Chem. 2007; 79:4900. [PubMed: 17530817]
10. a) Liu J, Lu Y. Angew Chem Int Ed. 2006; 45:90.b) Wang H, Yang R, Yang L, Tan W. ACS Nano. 2009; 3:2451. [PubMed: 19658387]
11. a) Dhar S, Gu FX, Langer R, Farokhzad OC, Lippard SJ. Proc Natl Acad Sci USA. 2008; 105:17356. [PubMed: 18978032] b) Zhu GZ, Meng L, Ye M, Yang L, Sefah K, O'Donoghue MB, Chen Y, Xiong XL, Huang J, Song EQ, Tan WH. Chem Asian J. 2012; 7:1630. [PubMed: 22492537] c) Farokhzad OC, Cheng JJ, Teply BA, Sherifi I, Jon S, Kantoff PW, Richie JP, Langer R. Proc Natl Acad Sci USA. 2006; 103:6315. [PubMed: 16606824]
12. a) Xiao Z, Levy-Nissenbaum E, Alexis F, Lupták A, Teply BA, Chan JM, Shi J, Digga E, Cheng J, Langer R, Farokhzad OC. ACS Nano. 2012; 6:696. [PubMed: 22214176] b) Bamrungsap S, Chen T, Shukoor MI, Chen Z, Sefah K, Chen Y, Tan W. ACS Nano. 2012; 6:3974. [PubMed: 22424140] c) Yu MK, Kim D, Lee IH, So JS, Jeong YY, Jon S. small. 2011; 7:2241. [PubMed: 21648076]
13. a) Shi D, Bedford NM, Cho HS. small. 2011; 7:2549. [PubMed: 21648074] b) Yu MK, Park J, Jon S. Theranostics. 2012; 2:3. [PubMed: 22272217] c) Kim J, Piao Y, Hyeon T. Chem Soc Rev. 2009; 38:372. [PubMed: 19169455]
14. Ma LL, Feldman MD, Tam JM, Paranjape AS, Cheruku KK, Larson TA, Tam JO, Ingram DR, Paramita V, Villard JW, Jenkins JT, Wang T, Clarke GD, Asmis R, Sokolov K, Chandrasekar B, Milner TE, Johnston KP. ACS Nano. 2009; 3:2686. [PubMed: 19711944]
15. a) Bagalkot V, Farokhzad OC, Langer R, Jon aS. Angew Chem Int Ed. 2006; 45:8149.b) Bagalkot V, Zhang L, Levy-Nissenbaum E, Jon S, Kantoff PW, Langer R, Farokhzad OC. Nano Lett. 2007; 7:3065. [PubMed: 17854227]

16. Wang AZ, Bagalkot V, Vasilliou CC, Gu F, Alexis F, Zhang L, Shaikh M, Yuet K, Cima MJ, Langer R, Kantoff PW, Bander NH, Jon SY, Farokhzad OC. ChemMedChem. 2008; 3:1311. [PubMed: 18613203]
17. Kim D, Jeong YY, Jon S. ACS Nano. 2010; 4:3689. [PubMed: 20550178]
18. Liang GH, Cai SY, Zhang P, Peng YY, Chen H, Zhang S, Kong JL. Anal Chim Acta. 2011; 689:243. [PubMed: 21397080]
19. Gotfredsen CH, Schultze P, Feigon J. J Am Chem Soc. 1998; 120:4281.
20. Seferos DS, Giljohann DA, Rosi NL, Mirkin CA. ChemBioChem. 2007; 8:1230. [PubMed: 17562553]
21. Chen T, Shukoor MI, Wang R, Zhao Z, Yuan Q, Bamrungsap S, Xiong X, Tan W. ACS Nano. 2011; 5:7866. [PubMed: 21888350]
22. Xiao Z, Shangguan D, Cao Z, Fang X, Tan W. Chem Eur J. 2008; 14:1769. [PubMed: 18092308]
23. Yu MK, Jeong YY, Park J, Park S, Kim JW, Min JJ, Kim K, Jon S. Angew Chem Int Ed. 2008; 47:5362.
24. Xiao Z, Ji C, Shi J, Pridgen EM, Frieder J, Wu J, Farokhzad OC. Angew Chem Int Ed. 2012; 51:11853.
25. Sherlock SP, Tabakman SM, Xie L, Dai H. ACS Nano. 2011; 5:1505. [PubMed: 21284398]
26. a) Bamrungsap S, Shukoor MI, Chen T, Sefah K, Tan W. Anal Chem. 2011; 83:7795. [PubMed: 21888415] b) Perez JM, Josephson L, O'Loughlin T, Hogemann D, Weissleder R. Nat Biotech. 2002; 20:816.
27. Liu J, Lu Y. Nat Protoc. 2006; 1:246. [PubMed: 17406240]

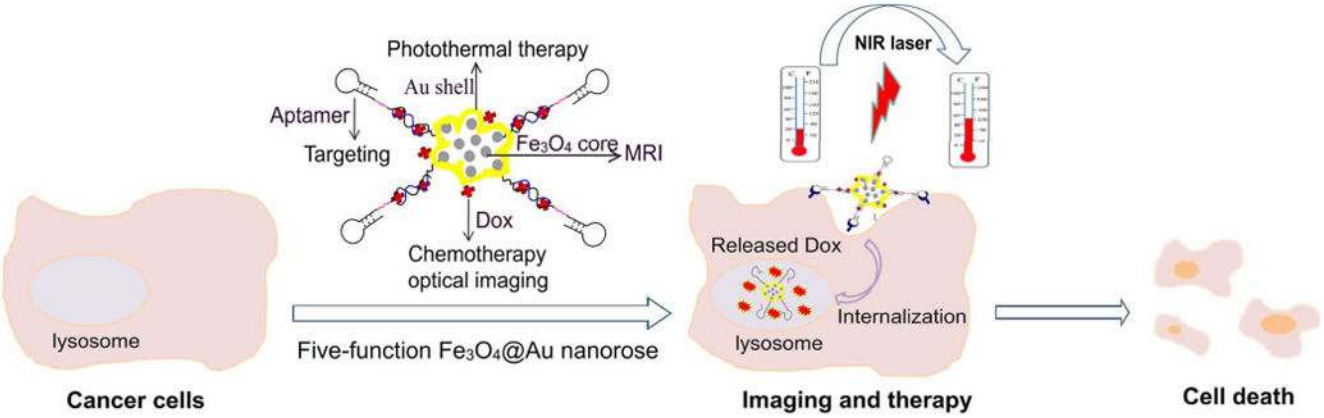

Figure 1.

Schematic representation of five-function Fe_3O_4@Au nanorose for cancer cell targeting, MRI, optical imaging, photothermal and chemotherapy. Sgc8 aptamers are conjugated on the surface of nanoroses for targeting of CCRF-CEM cancer cells. Anticancer drug (Dox) is specifically delivered into cancer cells for chemotherapy and optical imaging. Fe_3O_4@Au nanorose is an efficient MRI agent and photothermal agent; therefore, MRI and photothermal therapy can be achieved for cancer cell imaging and therapy.

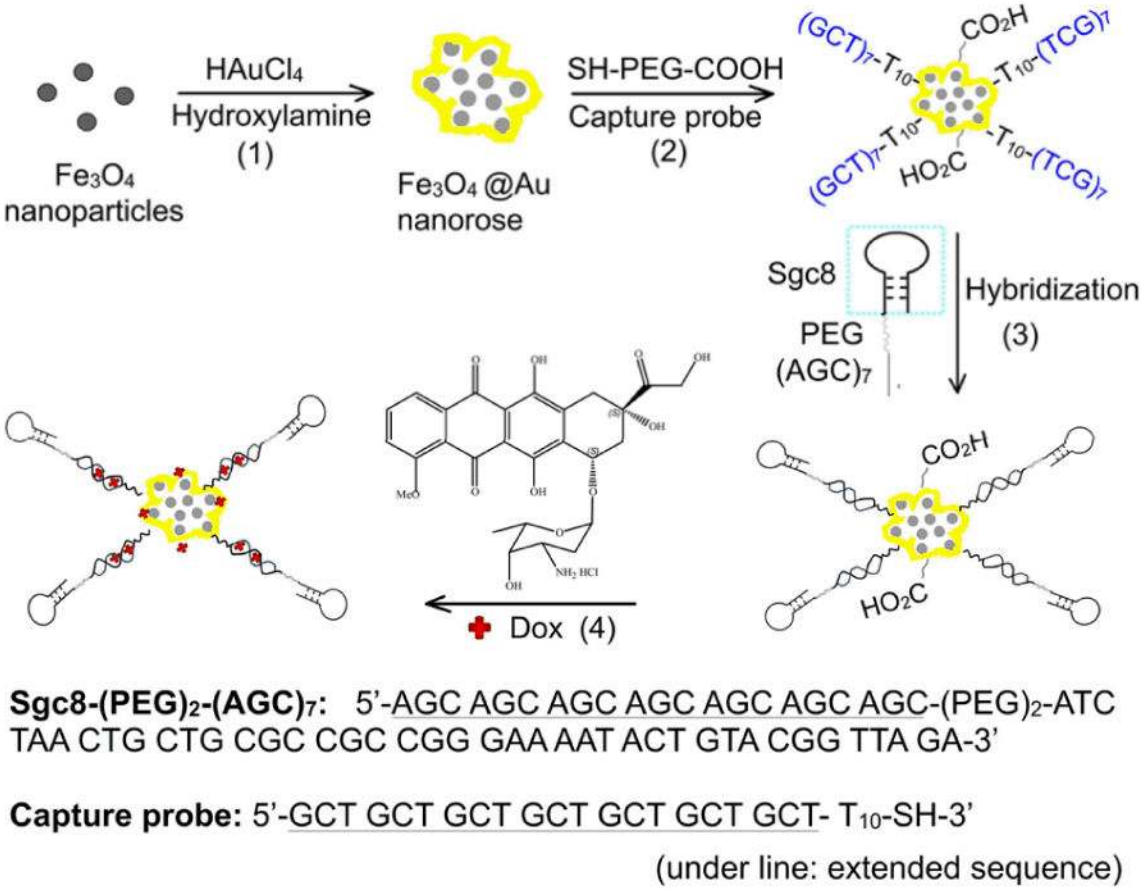

Figure 2.

Preparation of drug-loaded Fe_3O_4@Au nanorose. Fe_3O_4 nanoparticles were prepared first, followed by formation of nanoroses by the reduction of $HAuCl_4$ onto the surfaces of Fe_3O_4 nanoparticles. (2) A carboxylic acid-PEG derivative (SH-PEG-COOH) and a capture probe, 5′-$(GCT)_7$-T_{10}-SH-3′, were modified on the surface of nanoroses via gold-thiol bonds. (3) Sgc8 aptamer with a 21-base $(AGC)_7$ extension was hybridized with the capture probe to target CCRF-CEM cells and act as a carrier for Dox. (4) Dox is loaded on nanoroses through both intercalation into the extended GC base pairs and electrostatic interaction with the carboxyl groups on the nanorose surface.

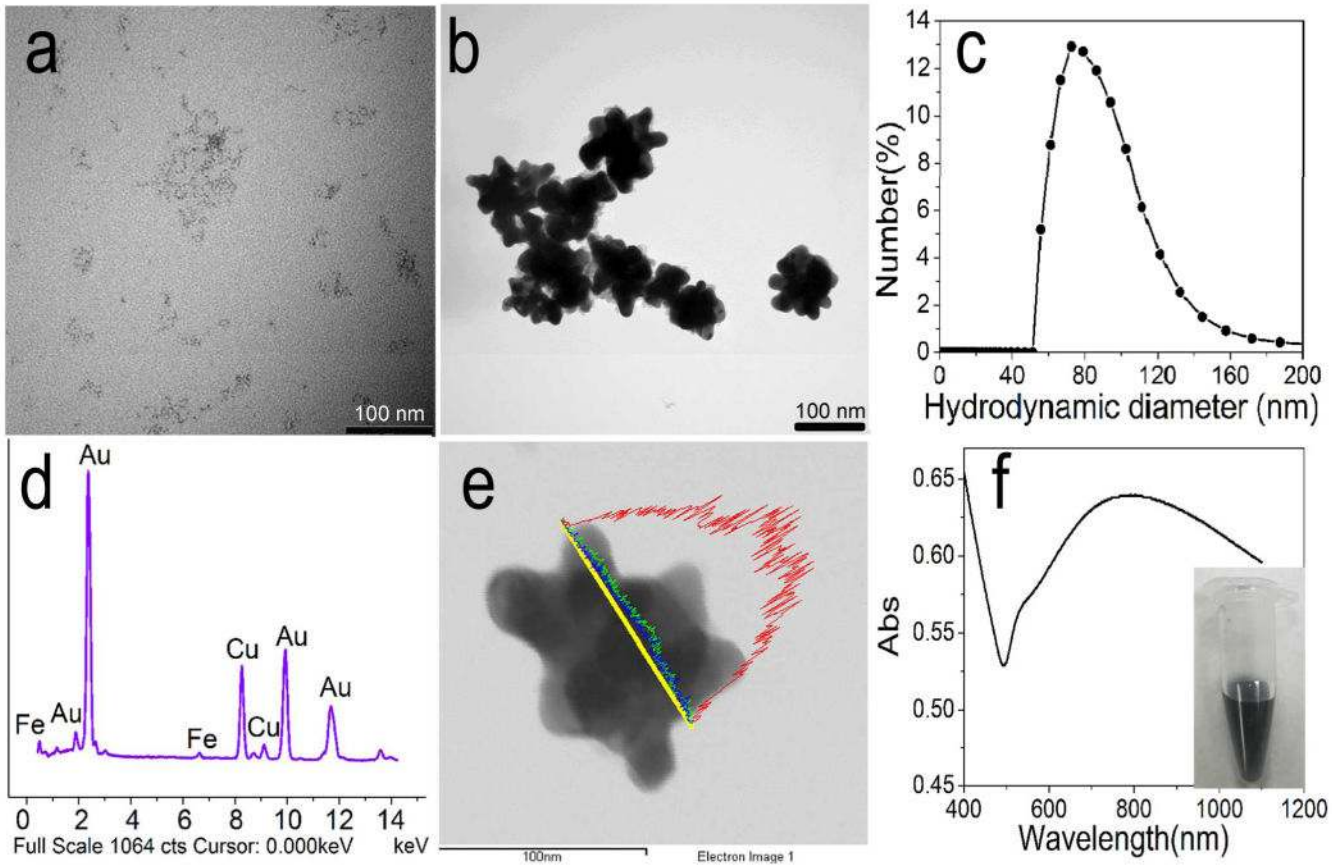

Figure 3.

Characterization of Fe_3O_4@Au nanorose. a, b, Transmission electron microscope (TEM) images of dextran-coated Fe_3O_4 nanoparticles (a) and nanoroses (b). Scale bar = 100 nm. c, Hydrodynamic diameter of nanoroses determined by dynamic light scattering (DLS) in Tris-HCl buffer (pH 7.5). d, e, Energy-dispersive spectroscopy (EDS) line scanning coupled with scanning transmission electron microscopy (STEM) from one nanorose. The outer surface line is from Au, and the lines throughout the cluster diameter are from oxygen and iron, respectively. Cu peaks are from TEM sample grid. f, UV-vis-NIR absorption spectra and solution color of nanoroses in Tris-HCl buffer (pH 7.5).

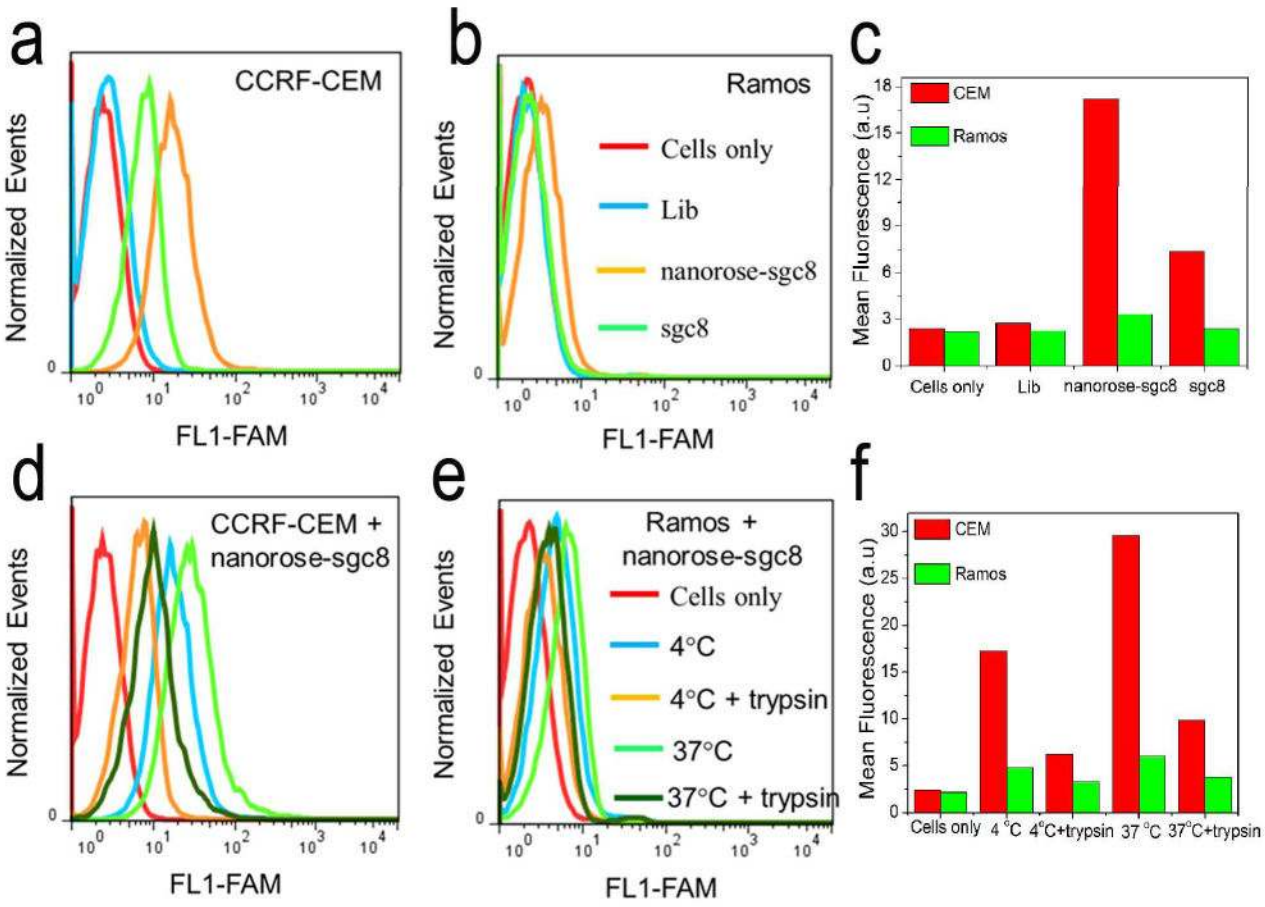

Figure 4.

Flow cytometry histograms to monitor the binding and internalization of free sgc8 and nanorose-sgc8 with CCRF-CEM and Ramos cells, respectively. a, b, curve 1 corresponds to cells only; curves 2, 3, 4 show cells incubated with lib, nanorose-sgc8 and sgc8 at 4°C for 30 min, respectively. c, mean fluorescence calculated from a and b. d, e, curve 1 corresponds to cells only; curve 2 and 4 show cells incubated with nanorose-sgc8 at 4°C for 30 min or 37°C for 2 h, respectively; curve 3 and 5 indicate trypsin treatment at 37°C for 10min was used after cells incubation at 4°C or 37°C, respectively. f, mean fluorescence calculated from d and e. CCRF-CEM or Ramos cells: 1×10^6 cells/mL. Free sgc8: 200 nM; sgc8 in nanorose-sgc8: 165 nM.

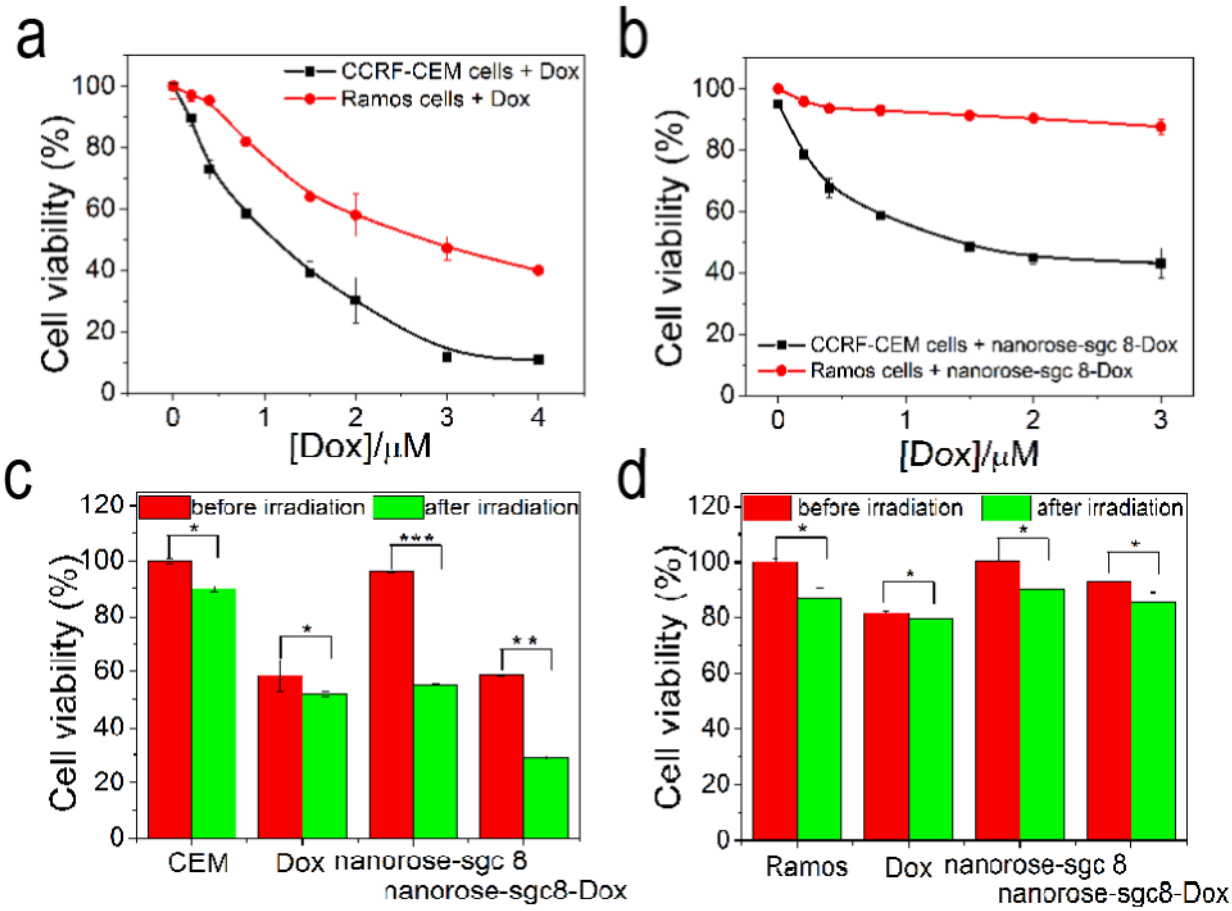

Figure 5.

Cytotoxicity assay of CCRF-CEM cells (target cells) and Ramos cells (control cells) treated with free Dox or nanorose-sgc8-Dox before and after NIR irradiation, respectively. a, b, CCRF-CEM cells and Ramos cells treated with free Dox (a) or nanorose-sgc8 (b). c, d, CCRF-CEM cells (c) and Ramos cells (d) treated with free Dox, nanorose-sgc8-only and nanorose-sgc8-Dox before and after NIR irradiation. NIR irradiation was conducted with an 810 nm continuous wave laser at 1.3 W/cm^2 for 10 min. CCRF-CEM or Ramos cells: 1×10^6 cells/mL. Dox: 0.8 μM. Nanorose-sgc8-Dox: 1.0 nM. *p* values were calculated by two-sample student's t-test.*$p < 0.05$, **$p < 0.01$, ***$p < 0.005$.

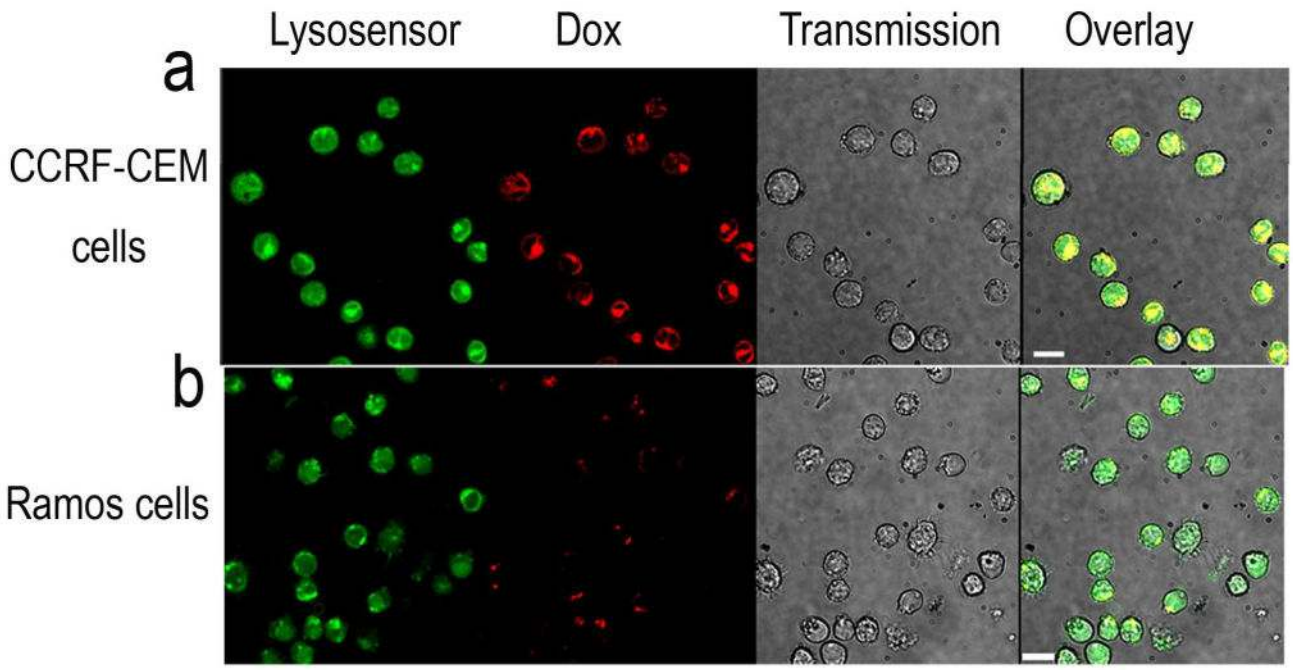

Figure 6.

Colocalization study of Dox released after incubation of nanorose-sgc8-Dox with CCRF-CEM cells (target cells, a) and Ramos cells (control cells, b). The first channel with green fluorescence is from LysoSensor; the second channel with red fluorescence is from Dox; the third channel is the transmission image, and the fourth channel is the overlay image of fluorescence and transmission. Scale bars = 10 μm. Cells were incubated at 37°C for 2h, followed by washing twice with washing buffer. CCRF-CEM or Ramos cells: 1×10^6 cells/mL. Nanorose-sgc8-Dox: 1.0 nM.

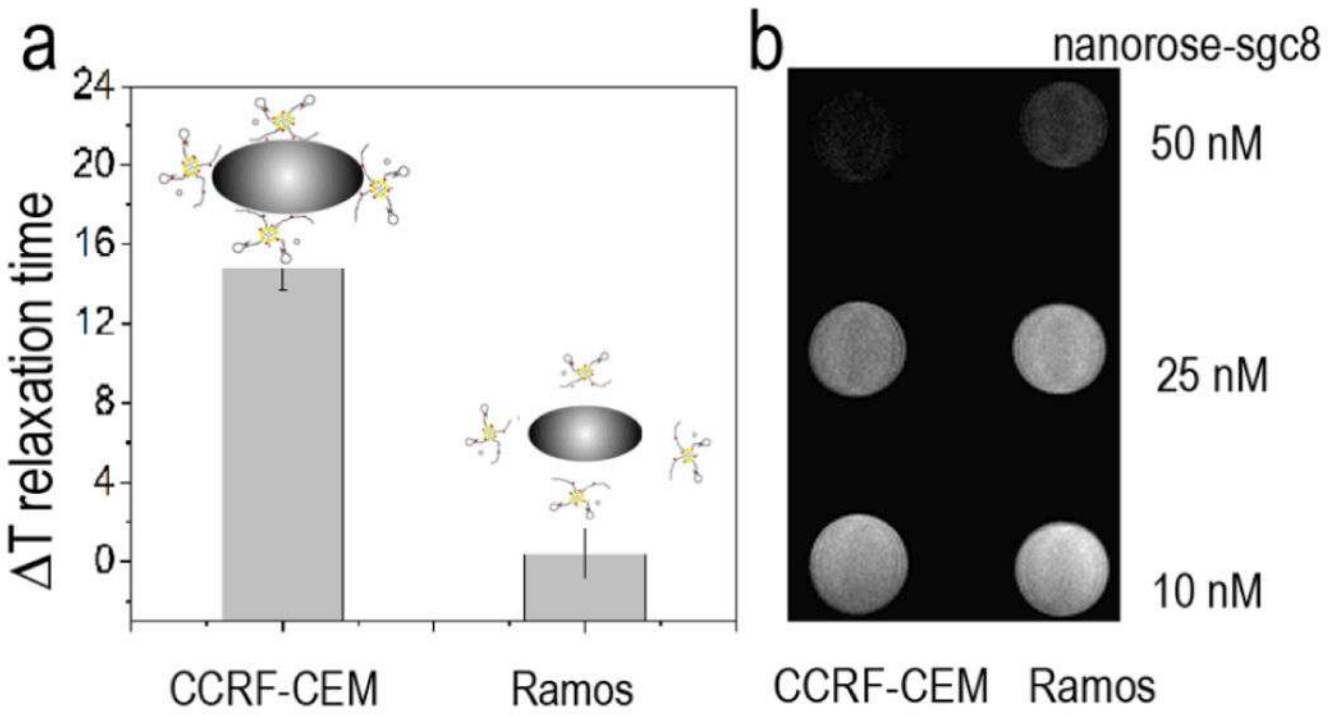

Figure 7.

Change in T_2 relaxation time and T_2-weighted MRI images of nanorose-sgc8 after incubation with CCRF-CEM cells (target cells) or Ramos cells (control cells). a) T_2 relaxation time change. b) T_2-weighted MRI images. CCRF-CEM or Ramos cells: 1×10^6 cells/mL. The concentration of nanorose-sgc8 in (a) is 25 nM, while concentrations in (b) are labeled on the right side of the figure.